QCD@Work 2003 - International Workshop on QCD, Conversano, Italy, 14–18 June 2003

QCD and Hadron Physics at CDF

Andrey Korytov (representing the CDF Collaboration)

Department of Physics, University of Florida, Gainesville, Florida, USA

Presented is a summary of the recent QCD and hadron physics results from the CDF collaboration.

1 Introduction

Results to be reported below are mostly based on the Run II data. To remind, CDF has undergone a number of major upgrades for the Run II, with a good fraction of the old CDF scrapped and replaced with brand new apparatus, designed to work at higher luminosity, providing better performance, and adding new capabilities. The CDF-II tracker can do the full track reconstruction, including 3D-vertex, in a much wider range $|\eta| \leq 2$, the calorimeters are hermetic up to $|\eta|$=5.1, the muon system covers the $|\eta|$-range up to 1.5. Another important upgrade is the added capability to trigger on the displaced vertices (b-tagging) and tracks with p_T >1.5 GeV/c. Tevatron center of mass energy in Run II is 1.96 TeV vs 1.8 TeV of Run I. As of May 2003, CDF has accumulated data corresponding to an integrated luminosity of about 130 pb^{-1}. However, many results to be presented will be based on somewhat smaller statistics.

It is impossible to cover in one talk all CDF analyses devoted to exploring various processes that one might refer to as the QCD and Hadron physics. At best, this report is only a glimpse on this broad on-going effort with the selection and organization of topics representing my personal preferences and views.

2 Hard QCD Physics

Hard QCD Physics at Tevatron is basically synonymous to measuring cross sections of processes involving high momentum transfers, i.e. production of jets (mostly gluons and light quarks), heavy flavor quarks (top, bottom, charm), and electroweak vector bosons (W, Z, γ). The perturbative methods can be and are used for calculating these cross sections. However, these calculations have been a long standing theoretical challenge due the large number of diagrams involved and often substantial uncertainties in the parton distribution functions (PDFs). E.g., fixed-order matrix elements for many of these processes are typically available at the Next-to-Leading-Order or even only at the Leading-Order. In addition, serious complications arise from the unavoidable ambiguities intrinsic to matching jets (experimental observables of varying definitions) with the fixed-order pQCD entities (a small number of quarks and gluons). The following subsections give examples of the forefront analyses in this domain. One should bear in mind that any significant deviations, if observed, may turn out to be manifestations of new physics.

2.1 Jets

Until the last year or so, the earlier Run I measurements of the inclusive jet cross section had been a controversial subject due to the apparent excess of events with high E_T jets as seen by CDF. Despite the fact that the observed departure from the theory was within the combined theoretical and experimental uncertainties, some argued that it might be due to quark compositeness or some other new physics. However, after the theoretical calculations were recently redone with the new set of PDFs released by the CTEQ collaboration (CTEQ6M), the experimental and theoretical $d\sigma/dE_T$ distributions at high E_T limit now match each other very well (Fig.s 1, 2). Thanks to the higher center of mass energy in Run II, the inclusive jet cross section is now measured up to jet E_T ~550 GeV (cf. E_T ~400 GeV in Run I). However, one may notice that the data points at low E_T <100 GeV appear to sag below the theoretical curve by about 20%—although this deviation is within the systematic errors, it was not present in the Run I data. The work on re-evaluating the Run II systematic errors is in progress.

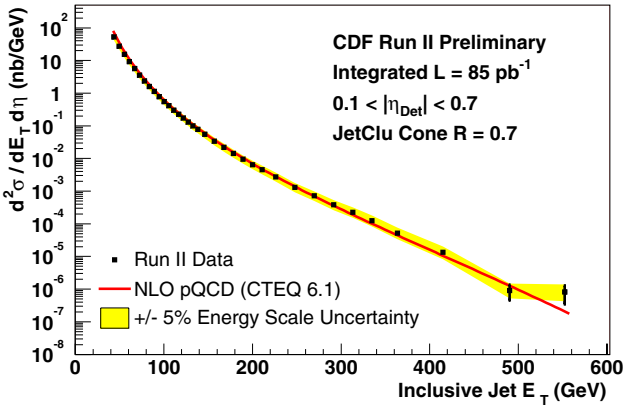

Figure 1. Inclusive jet cross section vs jet E_T

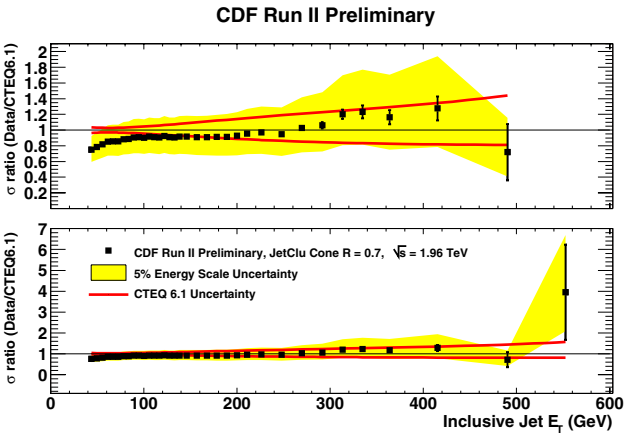

Figure 2. Inclusive jet cross section vs jet E_T: (Data-Theory)/Theory

The dijet mass distribution now has been measured up to M_{JJ} ~1.4 TeV (cf. 1 TeV in Run I), see Fig.3. This distribution was fit with a smooth line and checked bin-by-bin for excessive events in any of the bins, which might signal the presence of a narrow resonance. The current Run II 95% CL limits on the following narrow states have already exceeded the Run I results:

- o chiral color axigluons and extended Technicolor colorons are excluded in the mass range 200-1130 GeV,
- o excited quarks in the mass range 200-760 GeV,
- o color octet technirhos in the range 260-640 GeV,
- o superstring inspired E6 diquarks in the mass range 280-420 GeV.

The ratio of Run II to Run I dijet mass distributions agree with LO pQCD calculations within 10%. The angular dijet distributions for Run II are coming up soon.

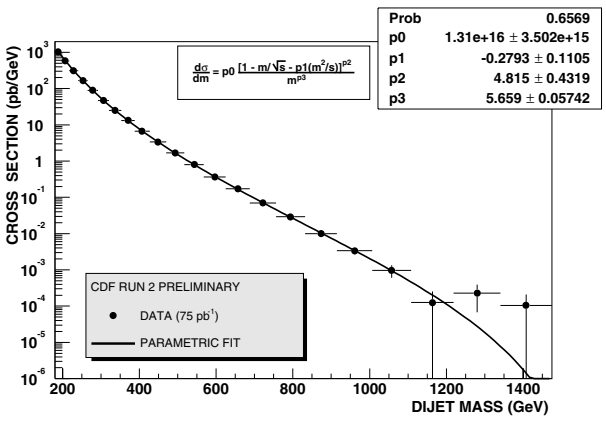

Figure 3. Dijet cross section vs dijet mass M_{jj}, GeV/c^2

2.2 Heavy flavor production

The top quark production is a plain pQCD process with the dominant contribution from gluon splitting. Fig.4 shows results of inclusive $t\bar{t}$-pair production cross section for Run I and Run II. One can see that Run II and Run I data agree with each other as well as with the theory. Of course, one might wish to see smaller experimental error bars, but this is a question of time or, more accurately, integrated luminosity.

The excess in b-quark production was a troublesome issue for a long time. E.g. the data/theory ratio in 2000 was ~2.9±0.5(exp)±0.5(theory). In 2002, however, the theory was revised by Cacciari and Nason: the NLO calculations were supplemented with NLL resummation and with the updated Peterson fragmentation function. The theoretical curve moved up and the data/theory ratio became ~1.7±0.3(exp)±0.5(theory), see Fig.5. The Run II results are forthcoming.

The direct charm quark production can be related to the number of direct D^0-mesons, identified via their decay mode $D^0 \rightarrow K^-\pi^+$. To do this analysis, the fraction of indirect D^0s coming from B-meson decays has to be removed. Taking advantage of the relatively long B-meson lifetimes, this fraction is evaluated from the tails in the reconstructed D^0-meson impact parameter distribution. The Run II results and the corresponding updated theoretical curve for D^0 are shown in Fig.6 and qualitatively look very similar to the case of the b-quarks from Run I (cf. Fig.5): the data points systematically go above the theory, but the discrepancy is well within the estimated experimental and theoretical uncertainties.

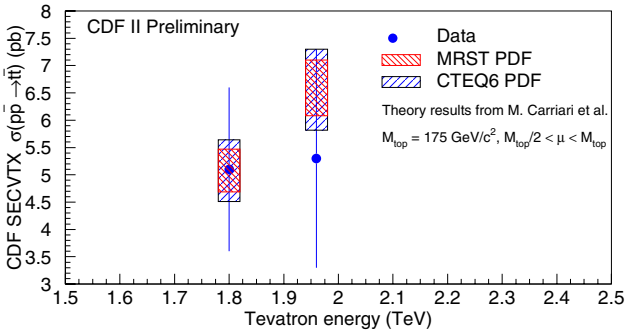

Figure 4. Inclusive $t\bar{t}$-pair production cross section at $\sqrt{s}$=1.8 and 1.96 GeV

2.3 W/Z/γ + jets cross section

Inclusive vector boson cross sections are a good probe of the pQCD physics that is free of the infamous jet finding/definition ambiguities. The W cross sections are known at the level of the NNLO for the inclusive production, NLO for W+1 jet, and LO level only for W + 2, 3,

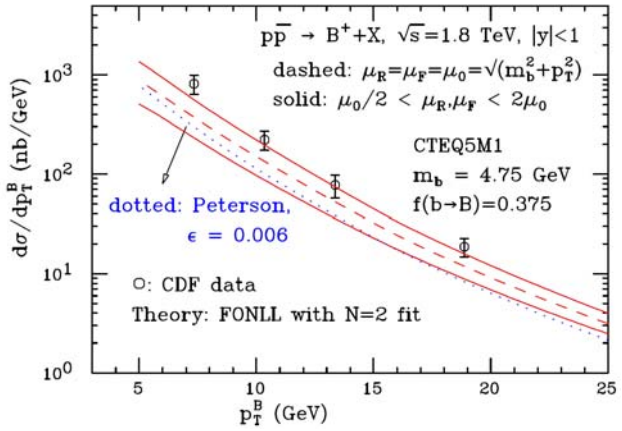

Figure 5. Differential B^+ production cross section at $\sqrt{s}$=1.80 TeV

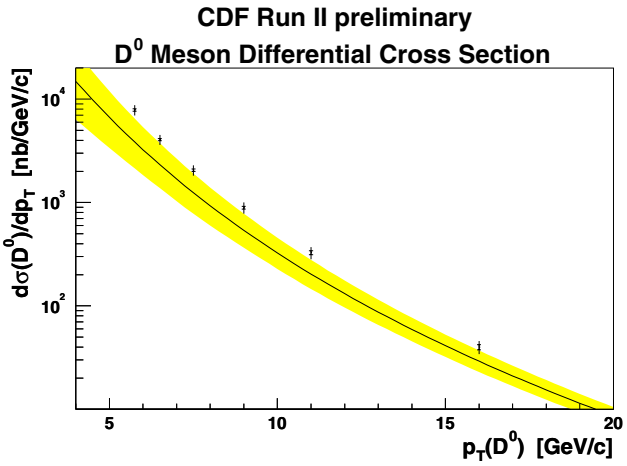

Figure 6. Differential D^0 production cross section at $\sqrt{s}$=1.96 TeV

4 jets. (MCFM does provide W+2 jets at NLO, but more work is needed to make it into an event generator.) Table 1 gives the measured inclusive cross sections in comparison to the corresponding LO, NLO, and NNLO theoretical calculations. The data agree well with both NLO and NNLO (the difference between NNLO and NLO is smaller than the current experimental uncertainties).

Table 1. Inclusive W production cross section (nb) in $p\bar{p}$ collisions at $\sqrt{s}$=1.80 and 1.96 TeV

	LO	NLO	NLLO	CDF Results
$\sqrt{s}$=1.80 TeV	1.76	2.41	2.50	2.38±0.24
$\sqrt{s}$=1.96 TeV	1.94	2.64	2.73	2.64±0.18

Analyses of W+jets, Z, γ production cross sections in Run II are in progress and results will become available in near future. Inclusive γ cross section is of particular interest due to the discrepancies in the steepness of the experimental and theoretical $d\sigma/dE_T$ distribution slopes seen in Run I.

3 Soft QCD and Hadron Physics

The domain of soft pQCD and hadron physics includes a variety of processes where characteristic momentum transfers are comparable to Λ_{QCD}: jet fragmentation (collective observables as well as formation of specific hadron species), structure of the underlying event in hard scattering processes, minimum bias events, diffractive processes, properties of specific hadrons (mass, lifetime, decay channels and their branching ratios). Some of these processes can be tackled by using various resumed pQCD approximations, lattice QCD calculations, and a number of phenomenological, often pQCD inspired, models that have been and are being developed for various specific cases. The measurements presented in the following subsections validate the approximations and assumptions used in these models.

3.1 Jet fragmentation

Earlier CDF studies showed that the momentum spectra of charged particles in jets with E_{jet} ~40-300 GeV could be well described by analytical formulas derived in the context of the Modified Leading Log Approximation. The new result is the analysis comparing quark and gluon jets. The CDF result is based on comparing jets in di-jet and γ-jet events that have very different fractions of quark and gluon jets. This approach minimizes possible experimental biases that might result from attempts to sort out quark/gluon jets on event-by-event basis. Also, we selected only central back-to-back jets and analyzed particle multiplicities in cones with small opening angles θ ($\sim 15-30^\circ$) around the jet axis, which allowed for a direct comparison to the theory.

Fig.7 and Fig.8 show the measured charged particle multiplicities in gluon and quark jets and their ratio vs. jet hardness scaling variable $Q = E_{jet}\theta$. Also, Fig. 7 shows 3NLLA fits, while Fig.8 shows predictions for the ratio as obtained in various Next-to-Leading-Log calculations. One can see that the data points in Fig.8 fall right on top of the recent pQCD calculations. Both figures also have some of the recent e^+e^- results, which are believed to be the least biased, both in terms of experimental methods used in sorting out light (u, d, s) quark and gluon jets and in terms of their reliance on theoretical models in extracting the value of the ratio (there are more than 10 independent LEP results ranging from r=1 to r=1.5).

3.2 Underlying event

CDF continues to pursue studies of the physics of the underlying event in hard collisions. The main processes

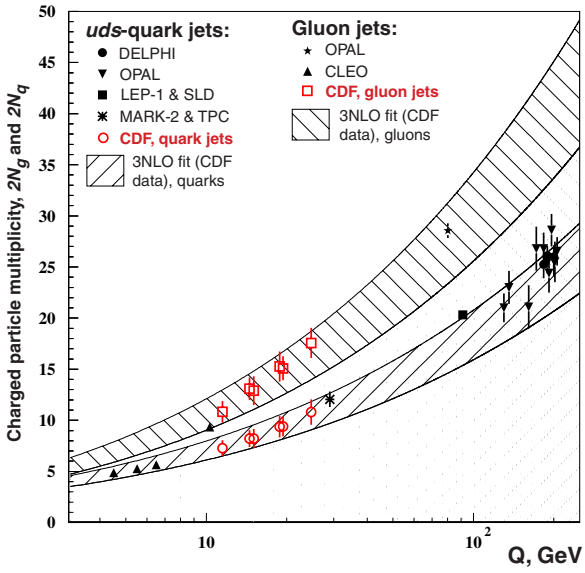

Figure 7. Multiplicities of charged particles in gluon and quark jets vs jet hardness $Q = E_{jet}\theta$ (see text). The CDF data is fit with 3NLLA (Capella et al, 2000)

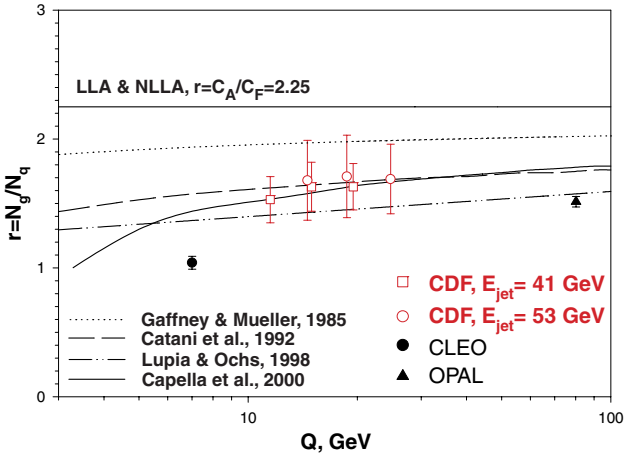

Figure 8. Ratio of average charged particle multiplicities in gluon and quark jets for dijet events. Particles are counted within an opening angle θ=0.28, 0.36, 0.47 *rad* around the jet direction and scale Q is defined as $Q = E_{jet} * \sin\theta$, where $E_{jet} = M_{jj}/2$.

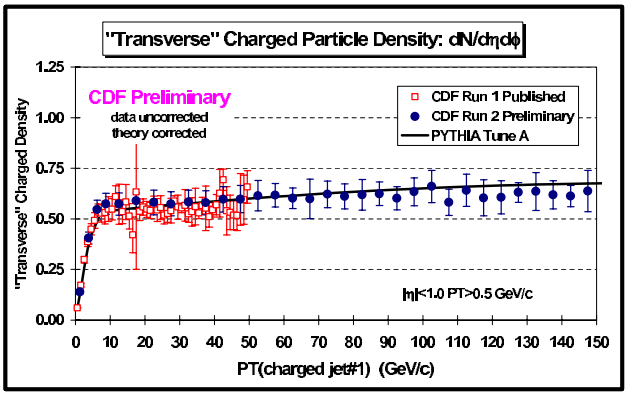

Figure 9. Average charged particle multiplicity flow density $dN/d\eta d\phi$ at η=0 and ϕ at 90° with respect to the leading jet as a function of the leading jet E_T

defining its structure are: proton-antiproton remnants, initial states radiation, and secondary parton interactions. Unfortunately, the only tool that we have in our disposal for these studies is a cross-comparison of the data and various Monte Carlo generators. By tuning the knobs made available in generators, we try to match the simulation to the data in the best possible way in order to gain deeper insights into the relative importance of the various contributing sub-processes.

Fig. 9 shows a remarkably good agreement of the data and tuned Pythia on the example of the charge particle multiplicity flow at η=0 in the ϕ-direction normal to the leading jet as a function of E_T of the leading jet. The other observables we monitored in the process of Pythia tuning were the average and differential energy flows in the direction normal to the leading jet. This excise shows that Pythia can be brought into a good agreement with data, but at the price of the following adjustments: the initial state radiation had to be significantly intensified; the dependence of the probability of multi-parton (secondary) interactions on the impact parameter had to be smoothed out; probability of di-gluon production in multi-parton secondary interactions had to be substantially enhanced over di-quark production and the probability of color connections of products of secondary interactions with $p\bar{p}$-remnants had to be increased. The work on comparing the data and Herwig is underway. Since the underlying event is modeled quite differently in Herwig, the comparison of what had to be tuned in Pythia and Herwig will help understand the roles of different sub-process and significance of the adjustments made to make Monte Carlo generators match the data.

3.3 Diffractive physics

The new Run II result is an extension of the earlier studies of the diffractive dijet production. Fig. 10 shows the measurement of the ratio of the single diffractive (SD) parton distribution function to that of the non-diffractive (ND) process $R = (\Delta\sigma_{SD}(x,\xi,Q^2)/\Delta\xi)/\sigma_{ND}(x,Q^2)$ for a range of ξ, the fraction of momentum lost by a scattered (diffracted) antiproton. Note that x for SD process can be taken as $x = \xi\beta$, where ξ is defined above and can be viewed as the fraction of antiproton momentum carried away by Pomeron, while β is the fraction of the Pomeron momentum carried away by one of its partons that ended up participating in the hard collision resulting in two jets, see Fig.10. Fig.11 shows a remarkable scaling, i.e. one can see that the ratio R is clearly ξ-independent in the range of 0.02< ξ <0.1. The ratio is also Q^2-independent in the range of 100< Q^2 <1600 GeV^2 (Fig. 12).

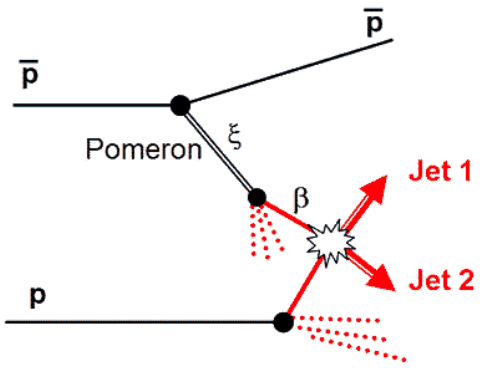

ξ = fraction of the antiproton momentum carried by Pomeron (defines the rapidity gap size)
β = fraction of Pomeron momentum carried by parton participating in hard scattering
x = β·ξ fraction of the antiproton momentum carried by a parton ended up participating in hard scattering
Q^2 (average E_T of two jets)^2

Figure 10. Difinition of single-diffractive dijet production variables (see text)

3.4 Physics of hadrons (masses, branching ratios, lifetimes)

Tevatron naturally provides us with enormous production rates of charm- and bottom-quark containing hadrons. The CDF-II with its extended 3D vertex coverage and the new secondary vertex trigger capabilities will collect very large samples of such hadrons. E.g., the current measurement of B_s mass, based on only L=70 pb^{-1}, is 5365.50±1.29±0.94 MeV (Fig.13), which is a noticeable improvement in comparison to the errors quoted in PDG2002 (5369.6±2.4).

Another new result is the improved limit on FCNC $D^0 \to \mu^+\mu^-$ branching ratio: BR$< 2.4 * 10^{-6}$ at 90% CL. This is an almost a factor of 2 better than the earlier best limit of $4.1 * 10^{-6}$. Note that the reconstruction of the $D^0 \to \pi^+\pi^-$ decays of almost identical kinematics provides an elegant way of evaluating systematic errors related to this search.

4 Conclusions

QCD and hadron physics drive a large number of phenomena that can be (and are being) observed and studied at Tevatron. The importance of these studies is two-fold. First, if there is a new physics to be observed at Tevatron, it is very likely to be produced via QCD-related processes and, therefore, may manifest itself in these studies. Second, there is an obvious need in refining the methods and tools used for theoretical calculations as well as in finding ways of reducing experimental systematic errors. Confronting data and theory and analyzing their consistency/disagreement from various points of views are the only means to facilitate advances in these areas.

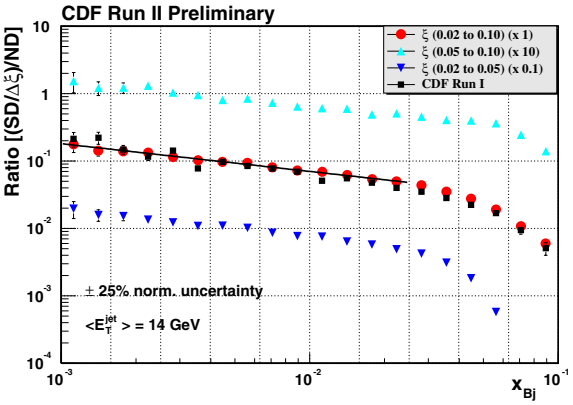

Figure 11. Ratios of single diffractive (SD) dijet cross section to that in a non-diffractive (ND) scattering vs Bjorken variable x and for different ranges of ξ, fraction of momentum lost by antiproton in the diffractive scattering

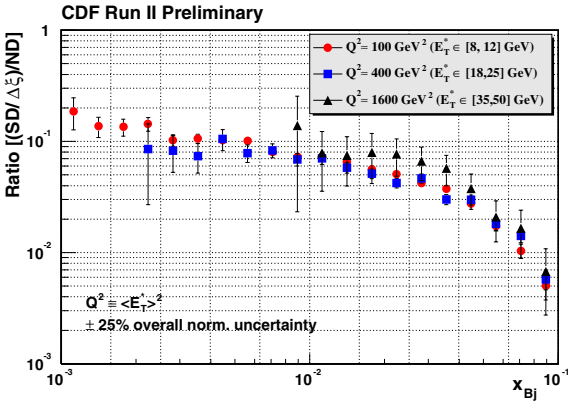

Figure 12. Ratios of single diffractive (SD) dijet cross section to that in a non-diffractive (ND) scattering vs Bjorken variable x and for different ranges of Q^2

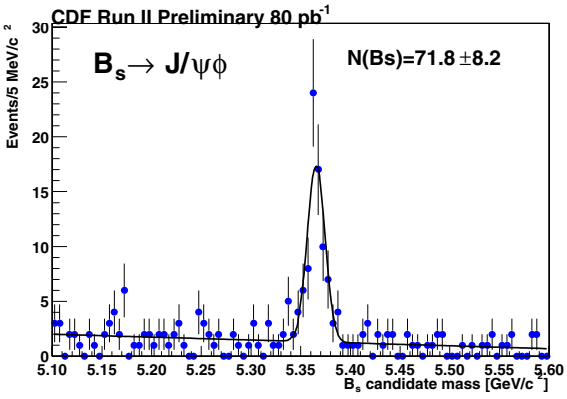

Figure 13. B_s mass distribution